SUMMARY OF BALLISTIC IMPACT DAMAGE IN TI-6AL-4V ALLOY WITH X-RAY COMPUTED TOMOGRAPHY

J.M.Wells[1], N.L.Rupert[2],W.H.Green[2], J.R.Wheeler[3], S.J.Cimpoeru[4] and A.V.Zibarov [5]
[1] JMW Associates, Mashpee, MA, USA; [2] US Army Research Lab. APG, MD, USA; [3]UCSC, Santa Cruz, CA,USA; [4]DSTO, Melbourne, Australia; and [5]GDT, Tula, Russia

Abstract: The in situ volumetric internal ballistic damage of monolithic Ti-6Al-4V alloy V_{50} targets was investigated using X-ray Computed Tomography, XCT. The interrogation was conducted with individual XCT scans of ~ 0.5 mm thickness to reveal 3D volumetric damage larger than the minimum feature resolution limits (> 0.25 mm). Image processing and visualization techniques utilized include contiguous 2D scan sequencing, reconstructed 3D solid objects and virtual sectioning, and colorized transparent point cloud imaging which clearly allows visualization of the volumetric damage network alone isolated from the opaque target material. Additionally, results of a new method to quantify the volumetric axi-symmetric damage fraction are shown. Observed internal damage features include multiple meso-scale cracks and voids. Of particular interest is the distinct and interesting meso-scale cracking morphology, described herein as "spiral orbital cracking", located beyond the penetration cavity in the exit half of the sample.

Introduction: In order to facilitate the development of light weight armor systems utilizing titanium alloys, one needs to establish improved methodologies for *in situ* characterization and visualization of the internal damage which occurs during ballistic impact. Too frequently, post-impact diagnostics have been mainly concerned with the extent of penetration and much less concerned with detail of the damage that surrounds the penetration cavity, both in instances of complete, as well as partial penetration. Ideally, it is desirable to predict *a priori* the nature, extent, and morphology of the impact damage in the Ti-6Al-4V target material following impact from threats of variable severity. It is also considered useful to have a demonstrated capability of actually characterizing the details of such impact damage to either verify or assist in the development of future predictive impact damage models.

The nondestructive technique of industrial X-ray Computed Tomography, XCT, is utilized by the authors [1-3] to significantly improve our diagnostic capabilities by providing the desired information to detect, locate, characterize, and visualize the impact damage in three dimensions (3D) in samples taken from impacted Ti-6Al-4V. targets. While destructive sectioning and polishing has the distinct traditional advantage of being able to observe target micro-structural and damage features at higher resolution levels than presently attainable with XCT. There are, however, several functional advantages of introducing XCT over destructive sectioning of ballistic impact targets including:

a) XCT is a ***reversible*** process using virtual sectioning where the target material can be restored and then repeatedly re-sectioned on arbitrary planes without consequences since no unintentional incipient damage is introduced into the sample during virtual mage processing. Also, the subject target retains its original pre-examination condition if desired for subsequent testing or evaluation.

b) Image processing software permits the virtual reconstruction of the digital XCT image into a variety of 2D multi-planar reconstructions and 3D solid objects, with arbitrary virtual sectioning and metrology applied as desired. Selected features such as voids or cracking networks can be virtually isolated and visualized in 3D as transparent point clouds entirely independent of the opacity of the original target material.

c) XCT provides a high resolution, non-destructive approach available to completely interrogate, capture and discriminate internal damage features throughout the entire 3D voxel volume of the target object. Resulting data can be stored and/or exported in several engineering formats. The initial ballistics study of the present Ti-6Al-4V alloy samples was described by Cimpoeru et al. [4]. Until recently, XCT technology had not been prominently utilized in the study of ballistic impact damage. DeLuca et al. [5] published an earlier study using XCT of impact damage in organic S2-glass reinforced polymer structural armor material. Wells, Green and Rupert [1, 2] reported on the use of XCT in the assessment of both pre- and post-ballistic impact damage in various armor ceramic materials including TiC, TiB2, Al2O3, and SiC and on the initial examination of these same Ti-6Al-4V samples [3]. The present work further develops this technique for improved 3D visualization and characterization of internal ballistic damage morphology in monolithic metallic target systems.

Results: Selected perforated samples of Ti-6Al-4V alloy were examined utilizing the 420 keV XCT facility at the ARL in Aberdeen Proving Ground, MD. Following initial digital radiographs revealing the through thickness profile of the penetration cavity, the XCT scanning of the samples was conducted perpendicular to the projectile flight direction from the impact face to the exit face in contiguous incremental slices of ~0.5 mm thickness. Macro-photograph images of the impact and exit faces are shown above their respective virtual 3D solid images of APM2 sample #2 (impact velocity 702 ms^{-1}) in Figure 1(a).

(a) (b)

Figure 1. (a) Macro-photographs of the 50 mm diameter AP<2 sample #2 (top) and the respective 3D XCT virtual object reconstructions (bottom) of both the impact (left) and (exit) surfaces, (b) Individual XCT axial scan #52 of Ti-6Al-4V APM2 sample #2 showing small damage voids and large curved orbital cracking segments. Axial slice is ~ 4 mm from the sample exit face.

Note that considerably greater detail is observed into the penetration cavity and in the topological surface features in the virtual images of the 3D XCT solid object reconstructions of both the impact and the exit surface than in the 2D macro-photographic images. In addition to the central penetration cavity, two basic meso-scale (> 0.25 mm) damage features are observed in the 2D XCT scan shown in Figure 1(b), namely scattered damage voids and prominent larger orbital cracking segments. These twodamage features appear ostensibly unconnected and lie predominantly in the lower half of impacted samples near the exit surface. When one observes these orbital cracking segments in a contiguous sequence of digitized XCT slice scans progressing in the direction toward the exit face as shown in Figure 2, the clockwise rotation of this damage feature becomes readily apparent. Similar results were obtained in all six of the APM2 Ti-6Al-4V alloy samples that were examined.

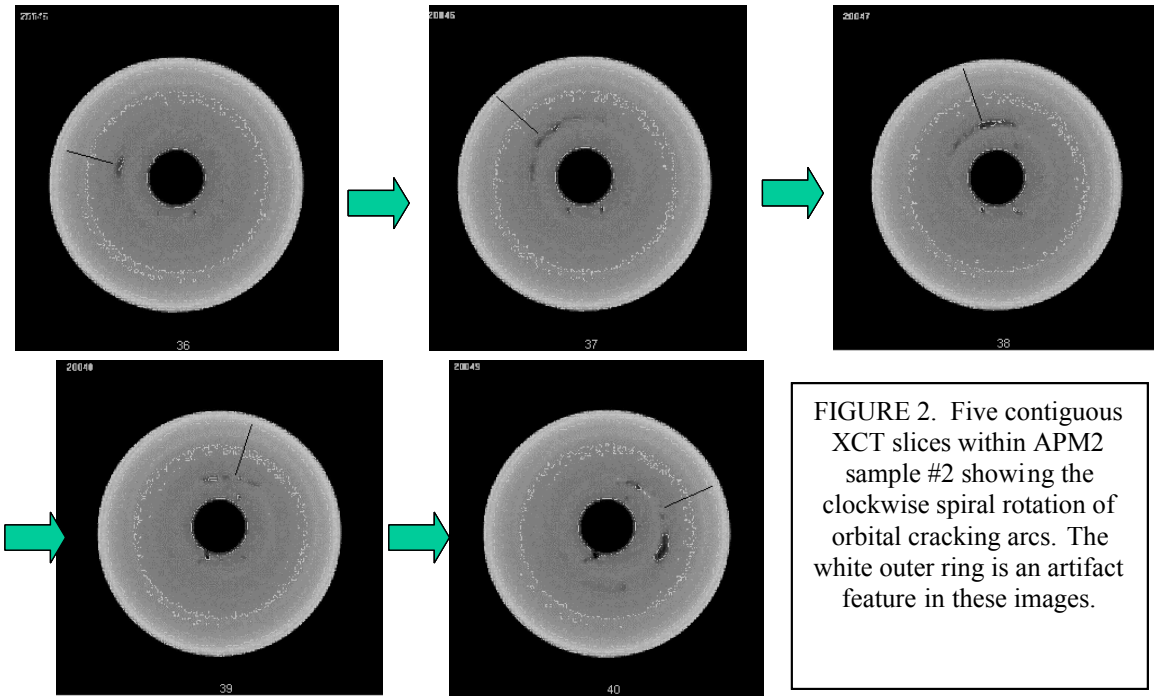

FIGURE 2. Five contiguous XCT slices within APM2 sample #2 showing the clockwise spiral rotation of orbital cracking arcs. The white outer ring is an artifact feature in these images.

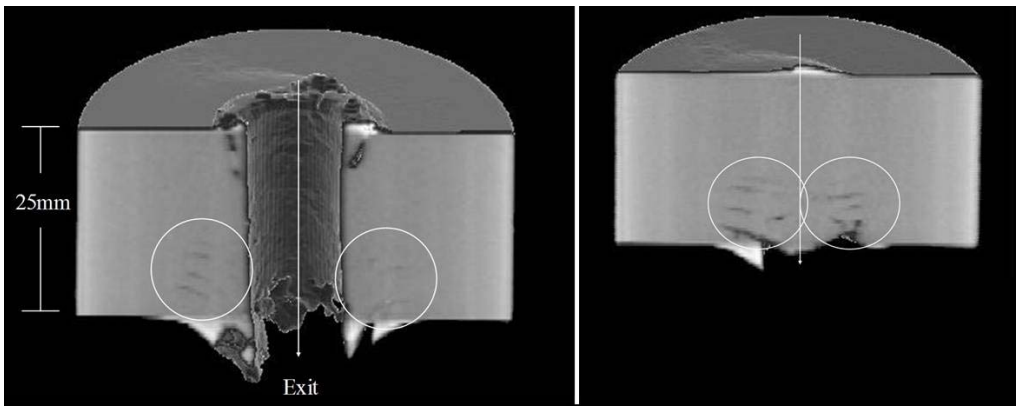

FIGURE 3. Virtual slices through a 3D solid object reconstruction of APM2 sample #2 showing ballistic damage beyond the cavity radius. Arrow indicates projectile direction from impact face (top) toward exit face (bottom) on center cut (left) and outer cavity radius cut (right) virtual sections.

Further details of the observed damage beyond the radius of the penetration cavity are revealed by virtual sectioning of the reconstructed 3D solid images of an individual sample. In this instance, arbitrary vertical slices are made parallel to the penetration cavity through the entire sample thickness. A series of such virtual slices was reconstructed from the XCT database at several selected radii from the center of the penetration cavity. Figure 3 reveals two such virtual slices, one through the approximate center and the second near the outer radius of the ballistic cavity in APM2 sample #2. Again, most of the observed damage of interest appears in the lower half of these figures near the exit face. The cracking features observed on both sides of the penetration cavity are shown in the circled areas and appear of several millimeters in length and with an orientation either as horizontal or slightly tilted downward toward the cavity center on the exit face.

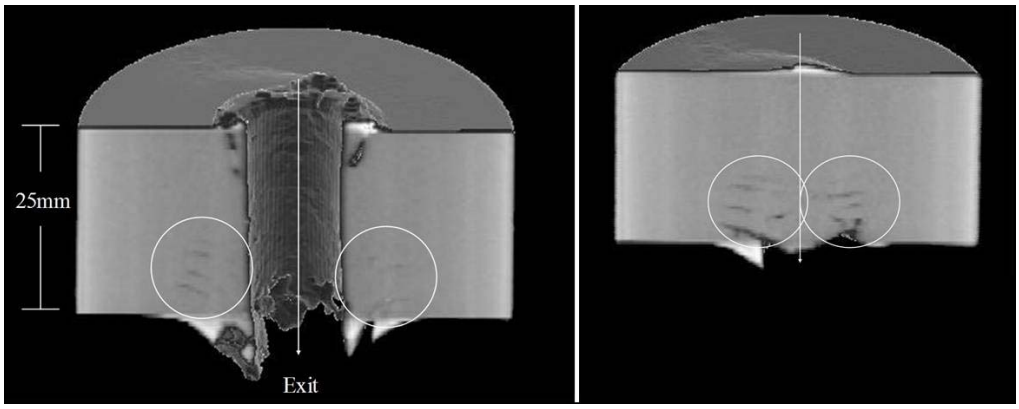

FIGURE 3. Virtual slices through a 3D solid object reconstruction of APM2 sample #2 showing ballistic damage beyond the cavity radius. Arrow indicates projectile direction from impact face (top) toward exit face (bottom) on center cut (left) and outer cavity radius cut (right) virtual sections.

Physical connectivity at a crack size less than the ~250 μm resolution achieved with XCT was observed in metallographic sections of the same sample, that were polished and etched (using a Nitric Acid/HF enchant). Full grinding, polishing and etching of the specimen in the direction of penetration was accomplished at DSTO in sequential 1 mm steps starting at the exit face. Each resulting full cross sectional surface was polished to 1200 grade paper and lightly etched and photographed. Fig 4(a) and 4(b) show two magnifications of the axially-ground section at ~9 mm from the exit face. The cross-section shown of a separate sample #9 in Figure 4(c) reveals how the fracture surfaces orient and how the plastically deformed zone that contains the fracture

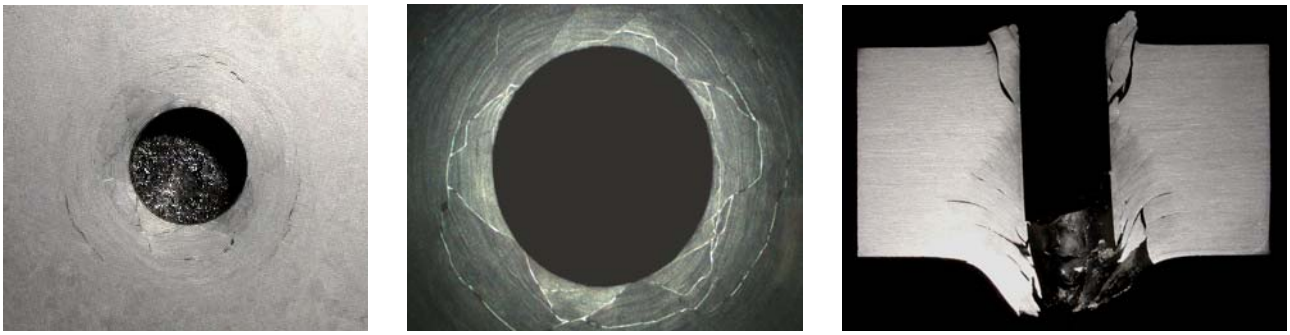

(a) (b) (c)

FIGURE 4. Images [3] of APM2 sample #2 (702 ms^{-1}) at a distance 9 mm from the exit face: (a), macro-photograph; (b) micrograph, showing shear bands and cracks connecting the meso-scale orbital cracks with the penetration cavity. A polished and etched cross section of APM2 sample #9 (682 ms^{-1}), (c) [3].

surfaces orient and how the plastically deformed zone that contains the shear bands appears to increase significantly in size as the exit face is approached. A plastic zone that increases in diameter with increasing penetration depth (to ~15 mm maximum radius) surrounds the penetration cavity. Interestingly, orbital cracking segments are observed at or near the outer boundary of the plastic zone. Shear bands in the plastic zone surrounding the penetration cavity, Fig 4(b), reveal that the crack segments are simply visible portions of shear failure connected by adiabatic shear bands.

Further processing of the entire sample XCT scan data file involved threshold segmentation and isolation of the damage data and reconstruction of virtual transparent point cloud images at ARL as shown in Fig 6. In this figure, one observes: (a) the radial extent of damage and (b) the localization of the orbital cracking outside of the penetration cavity as the exit face is approached. Additionally, one can observe clear indications of the spiral nature of the orbital cracking.

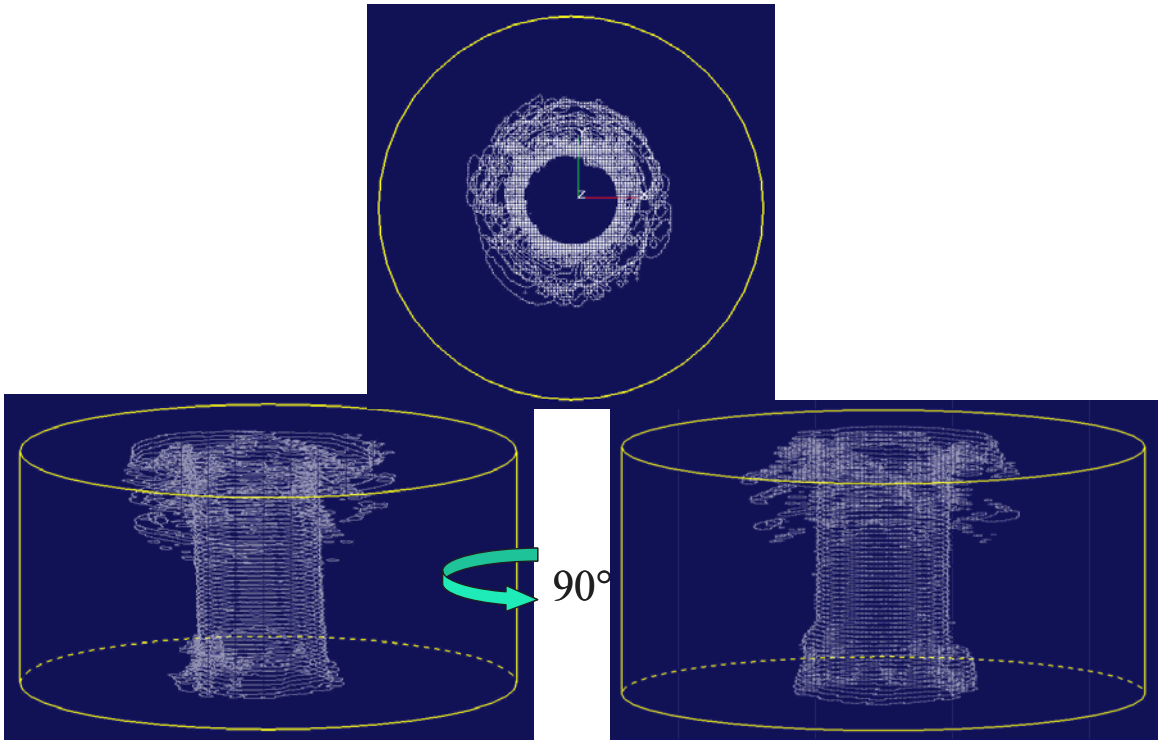

FIGURE 5. Transparent XCT point cloud images showing internal impact damage within APM2 sample #2 from top, front and side views. Exit face is at the top of the later images.

Additional virtual transparent point cloud images were reconstructed using GDT ScientificVR(c) visualizer software with more sophisticated variable 3D transparency and artificial colorization techniques that more clearly reveal the *in situ* orbital cracking morphology. These additional point cloud images are shown in Fig 6. The visualization of the impact damage of Fig 5 is considered to be further improved by reconstructing the threshold damage data using the GDT software, as shown in Fig 6. The artificial colorization is employed to assist in the depth registry of the observed features in these 2D images of 3D structures.

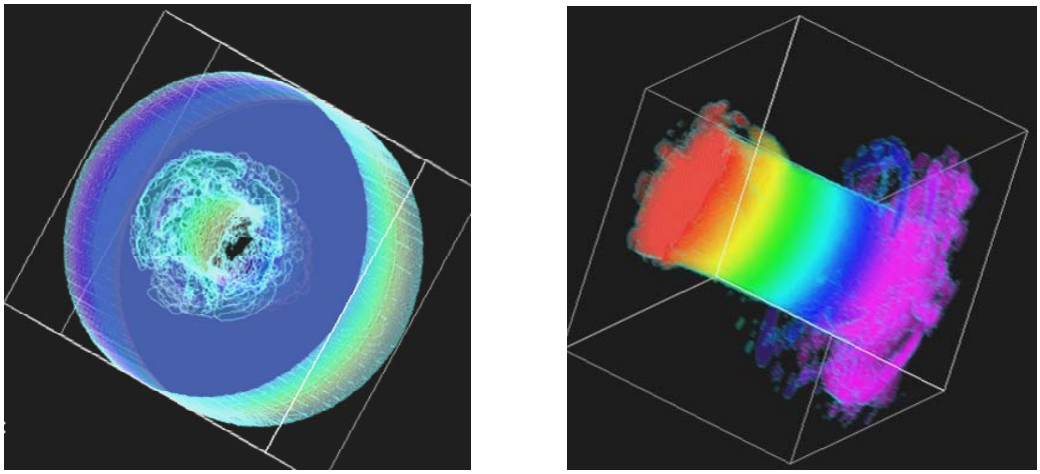

(a) (b)

FIGURE 6. Transparent Point cloud images from GDT Software Group showing internal impact damage within APM2 sample #2; (a) image shown with semi-transparent matrix and (b) fully transparent matrix.

Initial results of the quantification of the volumetric impact damage in sample APM2 #2 is shown in Fig 7. The axi-symmetrical damage fraction is plotted versus radius (in mm) from the center of the penetration cavity and along the entire penetration depth from the entrance to the exit face. The Z-axis labeled "Depth" is scaled according to the numerical sequencing of the XCT axial slices, starting with #10 at the impact face and #60 at the exit face of each APM2 sample (the depth of each slice is 0.5 mm thick). The Unit Damage Fraction parameter that is plotted as the ordinate can be defined as the normalized damage fraction measured as the fraction of damage pixels (actually voxels) in a toroidal ring from the edge of the penetration cavity out to the sample radius with the origin at the center of the cavity. These measurements are repeated for each axial slice through the entire axial scan data set. No account was made in this example of the angular orientation of the damage segments within each toroidal ring.

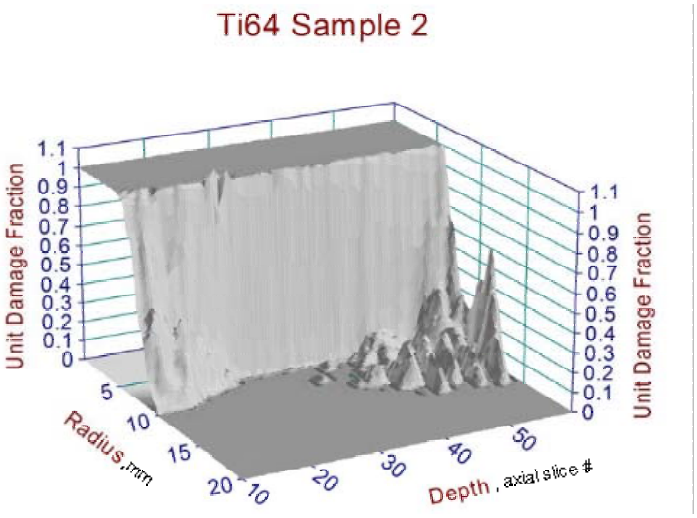

FIGURE 7. Quantitative 3D visualization of axi-symmetrical damage function in APM2 sample #2 plotted against radius and penetration depth data from the original XCT scans.

Discussion: The introduction of modern industrial X-ray computed tomography into the post-mortem process of ballistic impact damage characterization and analysis offers considerable advantages over prior more traditional approaches. Essentially such advantages include nondestructive 3D comprehensive volumetric damage visualization and quantitative characterizations as shown in figures 1-8 above. Traditional ballistic impact damage diagnostic methods include selective (and irreversible) destructive sectioning, nondestructive flash x-ray and visual external observations focused predominantly on penetration and dwell characteristics rather than target damage morphological details.

One benefit of using XCT for capturing the impact damage morphology is to gain new insight into damage details throughout the entire target sample volume that have previously been either under-investigated or, as in the case of the orbital spiral cracking, not been previously recognized and reported in the ballistic impact literature. It is important to note here that indications of this most interesting phenomenon of orbital spiral cracking now has also been observed by the present authors in two different ceramic ballistic target materials (TiC and TiB2).as well as in the current monolithic Ti-6Al-4V metallic alloy material. It is also obvious from the visualizations shown herein that the orbital spiral cracking is localized to the later stages of the penetration process in the Ti6Al-4V samples. In this case it is felt to be an apparent manifestation of a diecing failure mechanism [6] that forms due to fractures along various shear planes of weakness in the through thickness direction near the exit surface. The destructive metallographic sectioning of sample#2 was invoked only to establish the probable existence of a physical connectivity of the observed meso-scale cracking damage to the radius of the penetration cavity. Indeed, such a physical connectivity does exist at a scale below that of the present XCT methodology used.

Another benefit of capturing the volumetric impact damage details with the XCT nondestructive modality relates to its remarkable ability to provide direct 3D visualization and virtual metrology of the damage features of interest in situ and in a reversible or repeatable fashion. Keeping in mind the finite limits of resolution of ~ 0.5 mm or less, complex target assemblies can be examined, virtually sectioned, and have regions or features of interest completely

segregated and isolated from the host assembly matrix material(s) with the utilization of the transparent colorized point cloud techniques briefly demonstrated. Additionally, it has been shown feasible to quantify the normalized volumetric axi-symmetric damage fraction. Continuing developmental work should soon extend this capability to the asymmetrical case where the specific axial in-plane orientation of each damage feature will be incorporated as well. All of this ballistic impact damage information and visualization capability development is increasing the demands for improved relational data base knowledge management and scientific collaboration.

At present, no known ballistic damage modeling capability exists that has the demonstrated capability to predict the actual physical impact damage morphology observed in this study. If it were available, the authors hoped to use these results to verify the predictions of such a candidate model. However, in its present absence, the authors are attempting to work with various physical damage modeling approaches to assist in the development of future advanced predictive damage models and use the results such as those shown here to provide desirable physical verification of such future damage predictions.

Conclusions: The authors have provided several different 3D virtual images, as well as original 2D XCT scans, of ballistic impact damage in a monolithic Ti-6Al-4V alloy target. Beyond the through thickness penetration cavity, the most prominent and remarkable damage feature observed is that of a prominent orbital spiral cracking morphology concentrated to within ~ one projectile diameter of the target thickness near the exit face. This damage is constrained radially to within ~ three projectile diameters. While this damage appears to be physically unconnected to the penetration cavity in the XCT images, further detailed metallographic examination convincingly demonstrates fine scale physical connectivity that is below the resolution level currently available with XCT for samples of this size. Overall, the XCT scans and analysis have enabled a comprehensive visualization and understanding of both the failure mode and extent of damage in perforated monolithic Ti-6Al-4V targets. This will hopefully aid in the development and verification of advanced future predictive damage modeling techniques and also improve our understanding of the penetration resistance capability of this material.

References:

1. J.M. Wells, Green, W.H. and L. Rupert,, N.L. “Nondestructive 3-D Visualization of Ballistic Impact Damage in a TiC Ceramic Target Material”, *Proceedings MSMS2001, 2nd International Conference on Mechanics of Structures*, University of Wollongong, Wollongong, NSW, Australia, 14-16 159-165, 2001
2. J.M. Wells, N.L. Rupert, and W.H. Green, “Progress in the 3-D Visualization of Interior Ballistic Damage in Armor Ceramics”, *Proceedings of ACERS PacRim IV Conference*, Maui, Hawaii, 441-448, Nov. 2001
3. J.M. Wells, W.H. Green, N.L. Rupert, A. Cole, S.J. Alkemade, S.J. Cimpoeru and M. Szymczak, “Ballistic Damage Visualization in Monolithic Ti-6AL-4V with X-ray Computed Tomography”, *20th International Symposium on Ballistics*, Orlando, Fl, ADPA, Vol. 2, 1112-1120, 2002
4. S.J. Cimpoeru, S.J. Alkemade, M. Szymczak, N.L. Rupert, W.H. Green and J.M. Wells, “Ballistic Assessment of a Low-Cost Ti-6Al-4V Titanium Alloy”, *Australian J. of Mech. Engng*, 1, 5-9, 2003
5. E. DeLuca, J. Prifty, W , Betheney, and T. Chou, “Ballistic Impact Damage of S 2-Glass Reinforced Plastic Structural Armor”, *Composites Science and Technology*, 58, , pp. 1453-1461, 1998
6. R.L. Woodward, “The Interrelation of Failure Modes Observed in the Penetration of Metallic Targets”, *Int. J. Impact Engng*, 2, pp. 121-129, 1984